A new generation of anticancer, drug-loaded, colloidal vectors reverses multidrug resistance in glioma and reduces tumor progression in rats

Emmanuel Garcion,[1] Alf Lamprecht,[1] Béatrice Heurtault,[1] Archibald Paillard,[1] Anne Aubert-Pouessel,[1] Benoît Denizot,[1] Philippe Menei,[1,2] and Jean-Pierre Benoît[1]

[1]Institut National de la Santé et de la Recherche Medicale Unité 646 and [2]Département de Neurochirurgie, Unité de Thérapie Cellulaire, Centre Hospitalier Universitaire d' Angers, Angers, France

Abstract

By focusing on rat glioma, we elucidated whether new lipid nanocapsules (LNC) were able to improve anticancer hydrophobic drug bioavailability while also overcoming multidrug resistance. Blank LNCs and LNCs loaded with the antineoplastic agent paclitaxel were formulated by an emulsion inversion phase process. Expression of efflux pumps by rat glioma cells was assessed by reverse transcription-PCR, Western blot, and immunohistochemistry, and their activity was followed using the tracer $^{99}Tc^{m}$-methoxyisobutylisonitrile. Modalities of LNC action were addressed by using confocal microscopy detection of fluorescently labeled LNCs, fluorescence-activated cell sorting, high-performance liquid chromatography measurement of paclitaxel release, and analysis of tumor cell growth. This revealed an interaction between LNCs and efflux pumps that resulted in an inhibition of multidrug resistance in glioma cells, both in culture and in cell implants in animals. LNCs were able to target the intracellular compartment of glioma cells, a mechanism that was abrogated by using intracellular cholesterol inhibitors but not by clathrin-coated pit or caveolae uptake inhibitors. This result can be correlated to the LNC inhibitory effects on efflux pump activity that is itself known to be stimulated by intracellular cholesterol. In parallel, we showed that paclitaxel-loaded LNCs were active reservoirs from which paclitaxel could be released. Finally, we established that paclitaxel-loaded LNCs were more efficient than the commercially available paclitaxel formulation (Taxol) for clinical use, thus reducing tumor expansion *in vitro* and *in vivo*. Considering the physiologically compatible nature of LNC excipients, these data may represent an important step towards the development of new clinical therapeutic strategies against cancers. [Mol Cancer Ther 2006;5(7):1710–22]

Introduction

A pivotal issue in cancer chemotherapy is the development of drug delivery systems capable of optimizing the biotargeting of anticancer drugs in the body, at the same time as overcoming drug resistance mechanisms at the tissue and cellular levels.

One promising manner of addressing biotargeting is the employment of convenient submicronic colloidal systems that increase drug stability and improve drug distribution profiles, thus ameliorating the therapeutic index (1, 2). Although the recent expansion of nanotechnology has led to the emergence of different strategies, such as the use of drug-loaded liposomes (3–5), stealth liposomes (6, 7), polymeric nanospheres with equivalent stealth properties (8), polymeric nanocapsules (9), and solid lipid nanoparticles (10), a major obstacle to the success of chemotherapy in many cancers remains to be multidrug resistance (MDR).

Originally seen in cultured tumor cells, this phenomenon is likely to be multifactorial (e.g., the activation of detoxifying systems, DNA repair, and defective apoptotic pathways; ref. 11). However, it often results from the increased expression of ATP-dependent transporter proteins that drive the efflux of hydrophobic drugs from the cancer cells, thus lowering their intracellular concentration (11). In many MDR cell lines, the prototypic transporter responsible for this event has been identified as P-glycoprotein (MDR1; ref. 12). P-glycoprotein is a 170- to 180-kDa broad-spectrum multidrug efflux pump that belongs to a family of ATP-binding cassette transporters (11). Drugs that are affected by classic MDR include the *Vinca* alkaloids (vinblastine and vincristine), anthracyclines (doxorubicin and daunorubicin), the RNA transcription inhibitor actinomycin D, and the microtubule-stabilizing drug paclitaxel (11). As not all MDR cells express P-glycoprotein, a search for other efflux pumps was initiated, leading to the discovery of multiple MDR-associated proteins (11).

Because of the crucial implication of MDR in cancer chemotherapy, extensive efforts were made to design new

Received 5/17/06; accepted 5/23/06.

Grant support: Cancéropôle Grand-Ouest, Axe Vectorisation Tumorale d'agents diagnostiques et thérapeutiques, European Commission research grant QLK3-CT-2001-02226 for ''Biodegradable Controlled Drug Delivery Systems for the Treatment of Brain Diseases'' (E. Garcion and A. Aubert-Pouessel), Conseil Général du Maine et Loire (B. Heyrtault), Egide grant 316721F of the Région des Pays de Loire (A. Lamprecht), and Comité Départemental de Maine et Loire de la Ligue Contre le Cancer (A. Paillard).

The costs of publication of this article were defrayed in part by the payment of page charges. This article must therefore be hereby marked advertisement in accordance with 18 U.S.C. Section 1734 solely to indicate this fact.

Requests for reprints: Emmanuel Garcion, Institut National de la Santé et de la Recherche Medicale Unité 646, 10 rue André Boquel, 49100 Angers, France. Phone: 33-2-41-73-58-85; Fax: 33-2-41-73-58-53.
E-mail: emmanuel.garcion@univ-angers.fr

doi:10.1158/1535-7163.MCT-06-0289

P-glycoprotein inhibitors and novel drug delivery systems that can overcome MDR. As P-glycoprotein binds many different hydrophobic compounds, a large number of treatments have been described, which inhibit P-glycoprotein activity either by blocking drug binding, by interfering with ATP hydrolysis, or by altering the integrity of cell membrane lipids (13). In parallel, fatty acid ester surfactants, including Cremophor-EL, Triton X-100, and Tween 80, have been shown to interact with P-glycoprotein and to revert MDR (13). However, the use of most of these compounds is limited by their toxicity due to the high serum concentration that is required to inhibit P-glycoprotein. Moreover, as the majority of chemosensitizers are membrane-permeable molecules, minimal progress was made in the development of liposome formulations of MDR-reversing agents (14). Thus, synthetic block copolymer micelles [e.g., poly(D,L-lactide)-block-methoxy polyethylene glycol (PEG) or poly-(ethylene oxide)-block-poly(propylene oxide)-block-poly-(ethylene oxide); refs. 15–18] and poly(alkyl cyanoacrylate) nanoparticles (19–21) represent to date the most potent sensitizers of drug-resistant cancer cells. The inhibition of MDR by block copolymer micelles was attributed to the rapid incorporation to the cell membranes, spreading throughout the cells, and combined effects resulting in energy depletion and membrane fluidization (22). Reversal of MDR by poly(alkyl cyanoacrylate) nanoparticles was linked to simultaneous adhesion and degradation of the colloid to the cell surface. By taking advantage of the finding that Solutol HS15, which is a mixture of free PEG 660 and PEG 660 hydrostearate, reverts MDR and is biocompatible (23, 24), we here investigated the hypothesis that the new Solutol HS15-based formulation of lipid nanocapsules (LNC) developed in our laboratory (25–27) was able to improve anticancer drug delivery while also overcoming MDR. As malignant brain tumors represent a difficult therapeutic challenge in which MDR mechanisms play essential roles (28), the present study focused on rat glioma paradigms *in vitro* and *in vivo*.

Materials and Methods

Materials

The lipophilic Labrafac WL 1349 (caprylic-capric acid triglycerides, European Pharmacopeia, IVth, 2002) was provided by Gattefossé S.A. (Saint-Priest, France). Lipoïd S75-3 (soybean lecithin at 69% of phosphatidylcholine) and Solutol HS 15 were gifts from Lipoïd Gmbh (Ludwigshafen, Germany) and BASF (Ludwigshafen, Germany), respectively. Injectable solutions of verapamil at 5 mg/mL (Isoptine) and paclitaxel at 6 mg/mL (Taxol) were from Abbott France (Rungis, France) and Bristol-Myers Squibb (Rueil-Malmaison, France), respectively. Paclitaxel powder was from Indena (Milan, Italy). Injectable $^{99}Tc^{m}$-methoxyisobutylisonitrile ($^{99}Tc^{m}$-MIBI, Schering, Gif-sur-Yvette, France) was a kind gift from the Nuclear Medicine Unit of the University Hospital of Angers.

Formulation of LNCs and Preparation of Paclitaxel and Solutol HS15 Solutions

The overall study was made on 50-nm-diameter LNCs that were prepared according to the previously described original process (25). Briefly, Solutol HS15, Lipoïd, Labrafac, NaCl, and water (846, 75, 1,029, 89, and 2,975 mg, respectively) were mixed and heated under magnetic stirring up to 85°C. Three cycles of progressive heating and cooling in between 85°C and 60°C were then realized and followed by an irreversible shock induced by dilution with 12.5 mL of 0°C deionized water added to the mixture at 70°C. For the formulation of paclitaxel-loaded LNCs, 10 or 20 mg paclitaxel were first solubilized in a solution of 206 mg ethanol, 206 mg dichloromethane, and 10 mg cholesterol. Solutol HS15, Lipoïd, Labrafac, NaCl, and water were then added to this solution, and formulation of paclitaxel-loaded LNCs was done according to the above procedure with evaporation of dichloromethane and ethanol during the process. Photon correlation spectroscopy using a Malvern Autosizer 4700 (Malvern Instruments S.A., Worcester, United Kingdom) confirmed that all nanocapsules, loaded or not with paclitaxel, had a monomodal particle size distribution around 50.8 ± 0.1 nm and 53.9 ± 0.6 nm (mean ± SD), respectively, with a narrow distribution (polydispersity index <0.3). Solutions of Solutol HS15 (50 mg/mL), Taxol (containing 0.625 or 1.25 mg/mL paclitaxel), and Solutol HS15 plus Taxol were prepared in PBS.

Paclitaxel Stability

Paclitaxel was solubilized in the triglycerides usually forming the lipid material of the LNCs. This preparation underwent the heating and cooling cycles reported from the preparation procedure. Stability of the drug was obtained by comparing the results with nontreated paclitaxel-triglyceride solutions by high-performance liquid chromatography (HPLC) as previously described (29). Experiments were repeated in triplicate.

Determination of Drug Loading

For determination of paclitaxel encapsulation rate, LNCs were separated from supernatant using Centrisart C30 microcentrifuge filters (Sartorius, Goettingen, Germany). Paclitaxel concentration was measured in supernatant by HPLC in triplicate experiments, and the degree of encapsulation was calculated by consideration of initial amount of drug added.

In vitro Release Kinetics and Dissolution Study of Paclitaxel

In vitro release kinetic studies were done by dialysis; 2 mL of paclitaxel-loaded LNC suspension were filled into a dialysis tube (cutoff is 100 kDa) and inserted in a 100-mL flask containing 0.1 mol/L phosphate buffer saline added with 0.1% Tween 80 (PBST, pH 7.4) in a shaking water bath at 37°C at 75 rpm. At appropriate intervals, 0.5-mL samples were withdrawn, assayed for drug release, and replaced by 0.5 mL of fresh buffer. The amount of drug in the release medium was determined by HPLC as described above. To validate the release assay used, dissolution study of paclitaxel was conducted in PBST; 2 mL PBST were added to 2 mg paclitaxel powder in a 5-mL glass tube and

incubated at 37°C for 24 hours under gentle agitation with a SB1 Stuart Scientific tube rotator at 33 rpm (VWR International Merck Eurolab S.A., Fontenay-sous-Bois, France). Saturating solutions of paclitaxel were then collected and filtered on 0.2-μm Minisart syringe filters (VWR International) so as to remove non-soluble paclitaxel. Quantifications of paclitaxel were then made by HPLC coupled with tandem mass spectrometry as previously described (30). Experiments were made in triplicate. The saturating concentration for paclitaxel in PBST was observed to be 15.42 ± 2.37 μg/mL (mean ± SD). As it is higher than the maximum concentration that could have been obtained with 100% release of paclitaxel from LNCs (10.63 μg/mL), we here confirm paclitaxel solubility in PBST and validate the dialysis assay used.

P-glycoprotein LNC Interaction Assay

In vitro testing for LNC interaction with P-glycoprotein was made using a P-glycoprotein drug interaction assay kit according to the manufacturer's instructions (SpiBio, Massy, France).

Glioma and Newborn Rat Primary Astrocytes Cultures

Gliosarcoma 9L (9L) and glioma (F98) Fischer rat–derived cell lines were obtained from the European Collection of Cell Culture (Salisbury, United Kingdom) and the American Type Culture Collection (Manassas, VA), respectively. Purified newborn rat primary astrocytes were obtained by the mechanical dissociation method from cultures of cerebral cortex as originally described (31). The cells were grown at 37°C/5% CO_2 in DMEM with glucose and L-glutamine (Bio Whittaker, Verviers, Belgium) containing 10% FCS (Bio Whittaker) and 1% antibiotic and antimycotic solution (Sigma, Saint-Quentin Fallavier, France).

Fluorescent Labeling of LNCs

The fluorescent compound Nile red (Sigma) was used as described previously (32). Briefly, Nile red was dissolved in acetone at 1‰ (w/w), and the resulting Nile red solution was incorporated in the triglyceride phase (Labrafac) at 1:10 (w/w). LNCs were then prepared as above. A BD FACSAria fluorescent-activated particle sorter and the BD FACSDiva software (BD Biosciences, Le Pont de Claix, France) were used to determine the efficiency of the LNC labeling (cf. Results). To exclude potential interferences of free Nile red with Nile red–loaded LNCs during uptake experiments, PD10 Sephadex-G25 exclusion columns (Amersham Biosciences Europe, Orsay, France) were used to separate fluorescently labeled LNCs from possible free Nile red. As initial results with native fluorescent LNCs and purified fluorescent LNCs were found to be fully identical during the time experiments were made (data not shown), indicating complete encapsulation and retention of the fluorescent compound, all following work was made on native fluorescent LNCs.

Size Characterization of Nile Red–Loaded LNCs and Evaluation of Remaining Nile Red during Experimental Procedure

Photon correlation spectroscopy using a Malvern Autosizer 4700 confirmed that Nile red–loaded LNCs (LNC-NR) were similar to classic unloaded LNCs in size (51.17 ± 2.9 nm, mean ± SD) and in distribution (polydispersity index < 0.06). As LNC-NR were further used for characterization of LNC uptake by glioma cells, quantification of Nile red that remains loaded during experimental procedure was made after dialysis of LNC-NR in PBS (pH 7.4) at 37°C. For this purpose, 3 mL of a stock suspension of LNC-NR were filled into a dialysis tube (cutoff is 15 kDa) and inserted in a 50-mL beaker containing PBS (pH 7.4) maintained at 37°C under magnetic stirring at 75 rpm. After a 48-hour dialysis made in sink conditions (buffer solution withdrawn and replaced by fresh buffer at appropriate intervals), Nile red was extracted from LNCs by mixing 100-μL aliquots of the LNC-NR suspensions contained in the dialysis bag to 900 μL methanol. To remove LNC debris, samples were then centrifuged at 17,000 × *g* for 10 minutes, and Nile red concentrations (post-dialysis loading) were measured in supernatant by HPLC as previously described (33). The degree of remaining Nile red in LNCs was calculated by consideration of experimental determination of Nile red amount that was encapsulated for preparing LNC-NR stock suspension (pre-dialysis loading, considered as the 100% loading). Experiments were realized in triplicate.

Cellular Analysis of LNC Uptake by Flow Cytometry

A BD FACSCalibur fluorescent-activated flow cytometer and the BD CellQuest software (BD Biosciences) were used to perform flow cytometry analysis. Blank LNCs (LNC-Bl, 1:1,000), Nile red–loaded LNCs (LNC-NR, 1:1,000), or solutions of free Nile red prepared in water (from stock solutions in acetone) were incubated with glioma cells in serum-free medium containing 50% DMEM, 50% Ham's F12 (Bio Whittaker), and N1 complement (Sigma) at final concentrations of Nile red varying from 5.88 ng/mL (NRL-100 and LNC-NR, 1:1,000) to 0.588 pg/mL (NRL-0.01). After 2 hours of incubation, removal of attached LNCs was accomplished by washing the cells thrice (10 minutes) with 0.2 mol/L acetic acid/0.5 mol/L NaCl. Cells were then detached by trypsinization. After centrifugation, they were resuspended in a 0.4% (w/v) trypan blue solution in HBSS (Bio Whittaker) to quench the extracellular fluorescence (34), thus enabling determination of the fraction that was actually internalized. The treated samples were subsequently washed twice and analyzed by flow cytometry in at least triplicate experiments, with 3,000 to 10,000 cells measured in each sample.

Cellular Analysis of LNC Uptake by Confocal Laser Scanning Microscopy

F98 cells were plated at 10^4/mL in eight-well Lab-Tek Chamber Slides (Nunc, Roskilde, Denmark). After 24 hours of culture, they were washed with HBSS and incubated for 10 minutes to 2 hours (similar results obtained) in serum-free medium containing 50% DMEM, 50% Ham's F12, and N1 complement with LNC-Bl, LNC-NR, NRL-100, and NRL-100 with LNC-Bl. Cells were then fixed with 4% paraformaldehyde in PBS (pH 7.4), washed with HBSS

and finally mounted under coverslip in glycerol/PBS (1:1). Confocal microscope images were obtained by using an Olympus Fluoview FU 300 confocal laser scanning microscopy imaging system (Paris, France).

Cytoskeletal Disruption

The cells were preincubated with 10 mg/mL nocodazole (Sigma) for 60 minutes at 37°C to disrupt microtubules (35). Consecutively, LNCs were added and incubated in serum-free cell culture medium in the presence of the drug.

Cholesterol Depletion

Cholesterol depletion was carried out essentially as described previously (36). Accordingly, cells were treated with 10 mmol/L methyl-β-cyclodextrin (37, 38), in the presence of 1 mg/mL lovastatin (Sigma) for 1 hour at 37°C.

Potassium Depletion

Glioma cells were washed once with potassium-free buffer (pH 7.4) as described previously (39), containing 140 mmol/L NaCl, 20 mmol/L HEPES, 1 mmol/L $CaCl_2$, 1 mmol/L $MgCl_2$, 1 mg/mL D-glucose, followed by a wash with hypotonic buffer (potassium-free buffer diluted with water, 1:1). Then, the cells were washed again thrice with potassium-free buffer. Control cells were treated with buffer (pH 7.4) containing 140 mmol/L NaCl, 20 mmol/L HEPES, 1 mmol/L $CaCl_2$, 1 mmol/L $MgCl_2$, 1 mg/mL D-glucose, and 10 mmol/L KCl. LNCs were incubated with the cells in potassium-free or potassium-containing buffer, as indicated. Subsequently, the cells were analyzed by flow cytometry.

Treatment with Other Drugs/Inhibitors

Glioma cells were treated with chlorpromazine (10 mg/mL; ref. 40), nystatin (10 or 25 μg/mL; ref. 41), phorbol 12-myristate 13-acetate (1 or 10 μg/mL; ref. 41), or 5-(*N*,*N*-dimethyl)amiloride hydrochloride (10 mmol/L; ref. 42; all from Sigma), in serum-free culture medium for 1 hour at 37°C. Subsequently, LNCs were added, and the incubation was continued for another 2 hours, after which the cells were analyzed by flow cytometry.

Cell Survival Assay *In vitro*

Cells were first plated at 10^4/mL on plastic for 24 hours and then treated either with drug solution, blank, or drug containing LNCs of equivalent drug or excipient concentrations as assessed by paclitaxel stability and encapsulation rate in LNC. After 96 hours of incubation at 37°C/5% CO_2 and three washes in PBS (pH 7.4), cell survival (expressed as percentage of control untreated cells) was assessed by using the tetrazolium-based colorimetric 3-(4,5-dimethylthiazol-2-yl)-2,5-diphenyltetrazolium bromide assay. Absorbance measured at 570 nm is a function of the concentration of the converted dye, and the viable cell number is directly proportional to 3-(4,5-dimethylthiazol-2-yl)-2,5-diphenyltetrazolium bromide reduction (43).

Reverse Transcription-PCR

RNA from 9L or F98 cells was isolated using the Rneasy Mini kit (Qiagen S.A., Courtaboeuf, France) and reverse transcribed using First-Strand cDNA synthesis kit (Amersham Biosciences Europe). Oligonucleotides (10 pmol/L) were used for PCR reactions with a 5-minute denaturation step followed by 35 cycles of 1 minute at 95°C, 2 minutes at 58°C, and 2 minutes at 72°C and a final extension step at 72°C for 10 minutes. The primers used for amplification were designed based on Genbank sequences of the rat MDR1a, 5′-GGCCAGATGATCAAGACG-3′ (sense) and 5′-AACAAGTTGCTGTTCTGCC-3′ (antisense); rat MDR1b, 5′-AGTGACACTGGTGCCTCT-3′ (sense) and 5′-GTTACAATTCCGTTGTTTGG-3′ (antisense); rat MDR2, 5′-TGGCTGGAAAGCACGCAT-3′ (sense) and 5′-GCTTTACTGTGTCATCCC-3′ (antisense); and rat glyceraldehyde-3-phosphate dehydrogenase, 5′-TGAATGACATCAAGAAGGTGGTGGAG-3′ (sense) and 5′-TCCTTGGAGGCCATGTAGGCCAT-3′ (antisense).

Western Blots

Cells were washed twice with PBS and scrapped, and cell pellets were lysed in lysis buffer [50 mmol/L Tris-HCl, 5 mmol/L EDTA, 150 mmol/L NaCl, 1% Triton X-100, 2 mmol/L phenylmethylsulfonyl fluoride, 1 μg/mL pepstatin A, 2 μg/mL aprotinin, 5 μg/mL leupeptin (pH 7.4)] on ice for 30 minutes. Extracts were collected by centrifugation at 14,000 rpm for 10 minutes at 4°C. The amount of total soluble protein in the extracts was determined with the Bio-Rad detergent-compatible protein assay with bovine serum albumin as standard. For Western blotting, 20 μg of total proteins for each sample were then separated by SDS-PAGE and electroblotted onto nitrocellulose membranes (Hybond-P, Amersham Biosciences Europe). Membranes were blocked in 4% bovine serum albumin in TBS for 1 hour at room temperature. Blots were incubated with primary antibody overnight (C219 at 1:80 dilution; Clinisciences, Montrouge, France) at 4°C in 4% bovine serum albumin in TBS containing 0.1% Tween 20 (TBS-T) followed by a 2-hour incubation with the appropriate anti-mouse secondary peroxidase-conjugated antibody (Amersham Biosciences Europe) in TBS-T. The immunoreactive proteins were visualized using 3,3′-diaminobenzidine in TBS added with 0.03% H_2O_2.

Animals and Glioma Models *In vivo*

Syngeneic Fischer F344 male rats weighing 180 to 200g were obtained from Iffa Credo (L'arbresle, France). Animal care was given in strict accordance to European regulations. A cultured tumor monolayer was detached with trypsin-EDTA, washed twice with DMEM without FCS or antibiotics, counted, and resuspended to the final concentration desired. For both $^{99}Tc^m$-MIBI tumor uptake and tumor growth analysis, 100 μL of cell suspensions containing either 10^6 9L or F98 cells were injected s.c. into the left thigh of the rat. For i.c. implantations, 10^3 9L or 5×10^2 F98 cells were injected in the striatum of Fischer rats by stereotaxy at the following coordinates: 0.2 mm posterior from Bregma, 3.0 mm lateral from the sagittal suture, and 5.0 mm below dura as previously described (44).

Immunohistochemistry

Animals were killed on post-operative days 23 to 27 when they had severe clinical symptoms due to tumor evolution and were close from natural death. Brains were removed, frozen in isopentane at −30°C, and stored at −80°C; 14-μm frontal sections throughout the tumor were

made with a cryostat (Leica, Nussloch, Germany). Slices were then processed for immunohistochemical staining with washes in PBS (pH 7.4) between each step. They were dried for 30 minutes at room temperature, fixed with paraformaldehyde for 10 minutes at 4°C, and post-fixed with ethanol 95%/acetic acid 5% (v/v) for 5 minutes at −20°C. Sections were blocked in PBS/4% bovine serum albumin containing 10% normal goat serum and 0.1% Triton X-100 for 1 hour at room temperature and incubated overnight at 4°C with C219 or IgG2A isotype (BD Biosciences) primary antibodies at the concentration of 5.46 μg/mL in PBS/4% bovine serum albumin containing 0.1% Triton X-100. Slides were then incubated for 1 hour at room temperature with a rat-adsorbed biotinylated anti-mouse antibody (Vector, Burlingame, CA). Endogenous peroxidase activity was blocked by incubating the sections with 0.3% H_2O_2 for 15 minutes at room temperature, and color reaction was made using avidin-biotin complex kit (Vector) and incubation in PBS containing 3,3′-diaminobenzidine added with 0.03% H_2O_2. Finally, slides were slightly counterstained with toluidine blue and mounted with epoxide resin before optical microscope observation.

$^{99}Tc^m$-MIBI Cell Incorporation Assay

For *in vitro* assays, 9L or F98 cells were plated at 2×10^5 per 9-cm^2 well in 2 mL DMEM containing 10% FCS. After 24 hours of incubation at 37°C/5% CO_2, cells were treated with either verapamil, Solutol HS15, or LNC suspensions for 30 minutes at 37°C. $^{99}Tc^m$-MIBI (20 μCi) was then added to each well for 30 additional minutes at 37°C. Hence, cells were scrapped and separated from the supernatant by two centrifugations at 6,000 rpm in HBSS and finally resuspended 1 mL HBSS for gamma-counting at the energy window of 140 keV ± 20% (Cobra II, Packard Bioscience, Rungis, France). For *in vivo* $^{99}Tc^m$-MIBI uptake, 14 days after 9L or F98 cell implantation, animals were injected in the tumor mass with 100 μL of the different samples (PBS control, 2.5 mg/mL verapamil, 50 mg/mL Solutol HS15 solution, or 100 mg/mL LNCs containing 50 mg/mL Solutol HS15). Twenty-four hours later, 100 μCi of $^{99}Tc^m$-MIBI were injected i.v., and after 30 minutes, the rats were sacrificed. The tumor was removed and weighed, and the radioactivity content was measured by gamma-counting. As the mean verapamil elimination half-life in single-dose studies ranged from 2.8 to 7.4 hours, for verapamil groups, a second i.t. injection was made 1 hour before $^{99}Tc^m$-MIBI injection.

Analysis of F98 Tumor Progression *In vivo* and Statistical Analysis

F98-derived tumors formed a particularly even ellipsoid mass in the region of the injection site. Animals implanted s.c. with F98 cells were treated i.t. at day 5 after cell injection. For this purpose, F98-implanted animals were injected with PBS (control, $n = 7$), blank LNCs ($n = 7$), paclitaxel-loaded LNCs (Px-LNC, at the dose of 2.5 mg/kg body weight paclitaxel, $n = 9$), Taxol (paclitaxel, at the dose of 2.5 mg/kg body weight paclitaxel, $n = 8$), and Taxol with Solutol HS15 solution (paclitaxel + PEG-HS, at the dose of 2.5 mg/kg body weight paclitaxel and same amount of Solutol HS15 as the one contained in LNC, $n = 7$) in 400 μL. After killing the animals, F98-derived tumors were dissected and weighed. The length and width of each tumor were regularly measured using a digital caliper, and tumor volume was estimated with the mathematical ellipsoid formula (volume = $\pi/6 \times \text{width}^2 \times \text{length}$). Statistical significance in comparing tumor volume or tumor mass between groups for each experiment was determined by a Dunnett's test and by a Fisher's test.

Results

Expression of MDR Transporters by Glioma Cells *In vitro* and *In vivo* and Regulation of MDR by LNCs

To investigate MDR transport expression in our glioma cell models, reverse transcription-PCR analysis was used to detect the mRNA expression of P-glycoprotein members in 9L and F98 cells (Fig. 1A). Using gene-specific primers for MDR1a, MDR1b, and MDR2, MDR gene expression was detected in both 9L and F98 cells (Fig. 1A). To determine whether this gene expression of MDR transporters coincided with protein expression, a Western blot analysis was done using the monoclonal antibody C219, which recognizes a conserved COOH-terminal cytoplasmic sequence of P-glycoprotein isoforms. Our data showed that a 170-kDa band corresponding to P-glycoprotein isoforms is expressed at low level in primary rat astrocytes and increased with time in culture in both 9L and F98 rat glioma cells (Fig. 1B). By carrying out immunohistochemistry and using the C219 antibody in comparison to the isotype IgG2A, we also explored MDR transporters expression in intracranial tumors (Fig. 1C–H). We observed specific C219 immunolabeling in both 9L (Fig. 1C compared with Fig. 1F) and F98 (Fig. 1D compared with Fig. 1G) tumors. Such expression involved both the newly formed capillaries and the glioma cells themselves. In parallel, the C219 was able to stain specifically normal brain microvessels (Fig. 1E compared with Fig. 1H).

As MDR transporters were expressed *in vitro* and *in vivo* in our glioma models, we wanted to know whether our nanoparticulate systems could interact directly with these transporters and reverse MDR mechanisms. To address this issue, a P-glycoprotein drug interaction assay was carried out. This assay allows an *in vitro* screening for testing drug interaction with P-glycoprotein based on the modulation of ATPase activity from enriched P-glycoprotein inside-out membrane vesicle preparations (with P-glycoprotein intracellular domain facing the external compartment). As shown in Fig. 2A, we proved an interaction between LNCs with P-glycoprotein, which resulted in the negative regulation of ATPase activity and was comparable with the one observed with the known P-glycoprotein inhibitor vinblastin, whereas verapamil, another P-glycoprotein inhibitor, had a positive interaction on ATP hydrolysis.

Having established a direct interaction between LNCs and P-glycoprotein, examinations were carried out to see whether or not this finding resulted in some changes in the uptake of $^{99}Tc^m$-MIBI, a lipophilic cationic tracer that is also

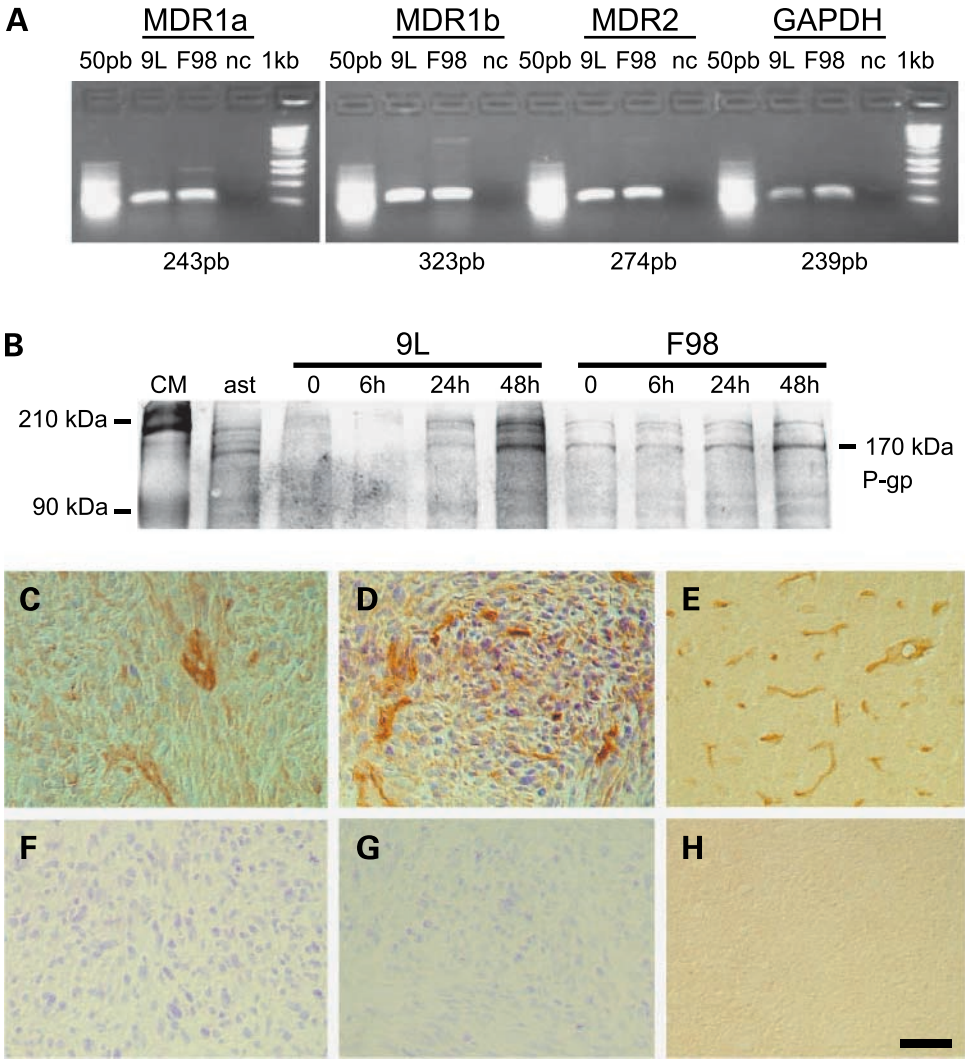

Figure 1. *In vitro* and *in vivo* expression of MDR transporters by glioma cells. **A,** reverse transcription-PCR analysis showing gene expression of *MDR1a*, *MDR1b*, and *MDR2* genes compared with glyceraldehyde-3-phosphate dehydrogenase (*GAPDH*) control in 9L and F98 cells 24 h after plating, with respective fragment sizes of 243, 323, 274, and 239 pair base (*pb*). *50 pb* and *1 kb*, size markers; *nc,* negative PCR control (no cDNA loaded during the amplification step). **B,** Western blot analysis with C219 antibody showing P-glycoprotein (*P-gp*) expression (size band of 170 kDa) in newborn rat primary astrocytes (*ast*), 9L, and F98 cells. Note the increased expression over time (0 – 48 h) after plating in both the cell line. **C** to **H,** immunohistochemical detection of P-glycoprotein (brown labeling) with slight toluidine blue counterstaining, in i.c. 9L (**C,** C219 antibody; **F,** IgG2A isotype) and F98 (**D,** C219 antibody; **G,** IgG2A isotype) rat glioma and in normal rat cortex microvasculature (**E,** C219 antibody; **H,** IgG2A isotype). Representative of three independent experiments.

a specific P-glycoprotein substrate, by 9L and F98 cells (45). Our data showed that after short exposure (30 minutes) to LNCs, at low dilution (1:1,000 and 1:100), the ability of cells to retain $^{99}Tc^{m}$-MIBI was significantly improved in both 9L (Fig. 2B, significance at 1:100 only) and F98 (Fig. 2C) glioma cells. Although the inhibitory effect was reduced in comparison with the one induced by verapamil at concentrations of 10 μmol/L, it was very similar to the one generated by Solutol HS15 at the respective concentration found in LNCs (1:1,000 and 1:100; Fig. 2B and C). This later result also attests that if Solutol HS15 is the main candidate involved in the inhibition of MDR by LNCs, its bioavailability is preserved in the drug delivery system under study. A similar investigation was then made *in vivo* 14 days after the implantation of tumor cells in rat thighs. Rats were treated i.t. with verapamil, Solutol HS15, or LNCs and, 24 hours later, received an i.v. injection of $^{99}Tc^{m}$-MIBI (100 μCi/200μL). Thirty minutes after this last injection, the animals were sacrificed; their tumor was removed; and their $^{99}Tc^{m}$-MIBI tumor incorporation was assessed by gamma-counting. As shown in Fig. 2D (9L glioma model) and Fig. 2E (F98 glioma model), treatment with LNCs significantly improved the uptake of $^{99}Tc^{m}$-MIBI *in vivo*. Although in the 9L glioma model both verapamil and Solutol HS15 had inhibitory effects (Fig. 2D), this was not the case in the F98 glioma model (Fig. 2E). This result emphasizes the fact that the modalities of MDR inhibition and its expression in glioma may differ from one cell type to another, and that LNCs represent useful MDR inhibitory objects.

Characterization of LNC Internalization/Endocytosis by Glioma Cells *In vitro*

To further investigate LNC-glioma cell interactions and better understand LNC effects on MDR, uptake of LNCs by 9L and F98 cells was investigated. For this purpose, LNCs were first labeled with Nile red as described in Materials and Methods. Fluorescent-activated particle sorting at 488 nm showed that 50-nm unlabeled LNCs displayed a low basal fluorescence (Fig. 3A). After Nile red incorporation, fluorescent-activated particle sorting at 488 nm showed

efficient LNC labeling with a Gaussian distribution of LNC numbers around a high-fluorescence intensity median (Fig. 3A). Thus, clusters of Nile red–stained LNCs can be visualized by fluorescent microscopy (Fig. 3B). To evaluate the amount of Nile red that remains loaded in LNC-NR during the experimental procedure, dialysis of LNC-NR in PBS (pH 7.4) at 37°C was completed for 48 hours in sink conditions. HPLC measurements in the dialysis bag showed that 96.20 ± 1.78% (mean ± SD) of the initially loaded Nile red remained encapsulated (Fig. 3C). Subsequently, mechanisms at the onset of LNC internalization by glioma cells were studied by incubating fluorescent LNCs for 2 hours with 9L or F98 cells. Evidence of LNC uptake was obtained by fluorescent-activated flow cytometry. To discriminate between cell association and actual internalization, extracellular fluorescence was quenched by addition of trypan blue, the non-quenched fraction thus representing internalized LNCs (34). As similar results were obtained with 9L and F98 cells, only data with F98 cells are presented. Examination of cells before (Fig. 3D, control) and after (Fig. 3D, LNC-NR) incubation with Nile red–stained LNCs revealed a marked increase in cell fluorescence intensity, thus showing rapid LNC uptake. As a consequence, mean cell fluorescence intensity before incubation with Nile red–stained LNCs was considered as 0% uptake and mean cell fluorescence intensity after 2 hours incubation as 100% uptake (Fig. 3D, histogram). To avoid any misinterpretation of the data, variation of Nile red uptake through cell fluorescence intensity was also investigated after glioma cell incubation for 2 hours with LNC-Bl or NRL solutions (from NRL-100 to NRL-0.01; cf. Materials and Methods). As expected, incubation of F98 glioma cells with LNC-Bl resulted in no increase of fluorescence intensity (Fig. 3D). More interestingly, although a slight Nile red uptake was seen when using NRL solution at 5.88 ng/mL (NRL-100), none was observed when using NRL solution at 0.294 ng/mL (NRL-5; Fig. 3D). Because this last concentration is yet higher than the maximum Nile red that can be released after 48 hours from LNC-NR in saline media (Fig. 3C), it can be asserted that the dye used cannot be transferred on its own to the cells during the 2-hour incubation with LNC-NR. This last point was also confirmed by confocal laser scanning microscopy experiments. As shown on Fig. 3E, Nile red staining of F98 glioma cells was only observed when using LNC-NR (note that the fluorescence pattern is more pronounced in a perinuclear area but avoiding the nucleus) and not when using NRL-100. Additionally, the use of LNC-Bl when treating the cells with NRL-100 did not resulted in any staining (Fig. 3E), thus showing that LNCs themselves cannot facilitate free Nile red to enter glioma cells. Therefore, when using LNC-NR, Nile red uptake by glioma cells can accurately be considered as LNC uptake. Investigation of energy-dependent cell uptake processes was made by using previously identified inhibitors of known endocytic pathways (cf. Materials and Methods). Variation of the basal mean fluorescence intensity after treatment with inhibitors was determined by flow cytometry at the 2-hour incubation time point. Our data, presented in Fig. 3F, revealed that microtubule disruption (nocodazole) did not affect LNC uptake. In contrast, cholesterol depletion (methyl-β-cyclodextrin and lovastatin), which has been shown to alter both clathrin-dependent and clathrin-independent cell uptake mechanisms (46–49), had a strong effect on LNC uptake by F98 glioma cells (about 75% reduction; Fig. 3F). To determine the relative participation of clathrin-dependent uptake mechanisms, chlorpromazine treatment (40) and potassium depletion (39) were used to specifically inhibit clathrin-coated pit formation and clathrin-dependent endocytosis. As shown on Fig. 3F, whereas a slight but nonsignificant decrease in LNC internalization was observed after chlorpromazine treatments (reduction of about 25%), no effects were seen with potassium depletion, indicating a relatively low implication of clathrin-coated pit formation in the uptake of LNCs by glioma cells. It was assumed that LNC endocytosis would be mediated through a clathrin-independent

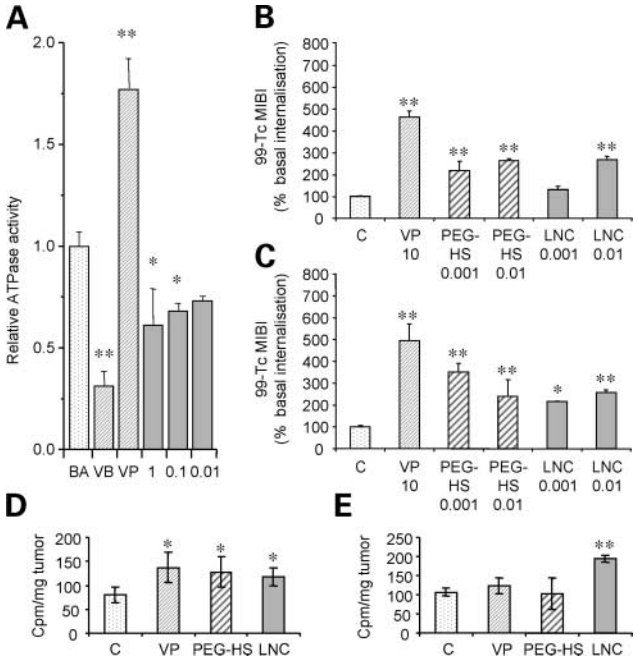

Figure 2. Interaction of LNCs with efflux transporters. **A**, *in vitro* screening of LNC interaction with P-glycoprotein–dependent ATPase activity using enriched P-glycoprotein inside-out membrane vesicle preparations. Note that as with vinblastine (*VB*) and verapamil (*VP*), LNCs modulate the basal relative ATPase activity (*BA*) at all dilutions tested [from pure (*1*) to 1:100 (*0.01*)]. **B** and **C**, $^{99}Tc^{m}$-MIBI uptake by 9L (**B**) and F98 (**C**) cells *in vitro*. Note that LNC, Solutol HS15 (PEG-HS), and verapamil at all concentrations tested improve intracellular retention of the surrogate tracer of MDR inhibition. **D** and **E**, modulation of MDR by LNC *in vivo*. 9L (**D**) and F98 (**E**) cells were implanted s.c. in Fischer rats and $^{99}Tc^{m}$-MIBI later injected i.v. $^{99}Tc^{m}$-MIBI tumor uptake was then assessed after tumor dissection and gamma-counting (cpm/weight of tumor). Note that i.t. treatment with both LNCs, Solutol HS15 (PEG-HS) and verapamil improve the intracellular retention of the surrogate tracer of MDR inhibition in the 9L model, whereas Solutol HS15 and verapamil are inefficient in reversing MDR in the F98 model. *Columns,* mean; *bars,* SD. **, $P < 0.01$; *, $P < 0.05$ (Dunnett's test).

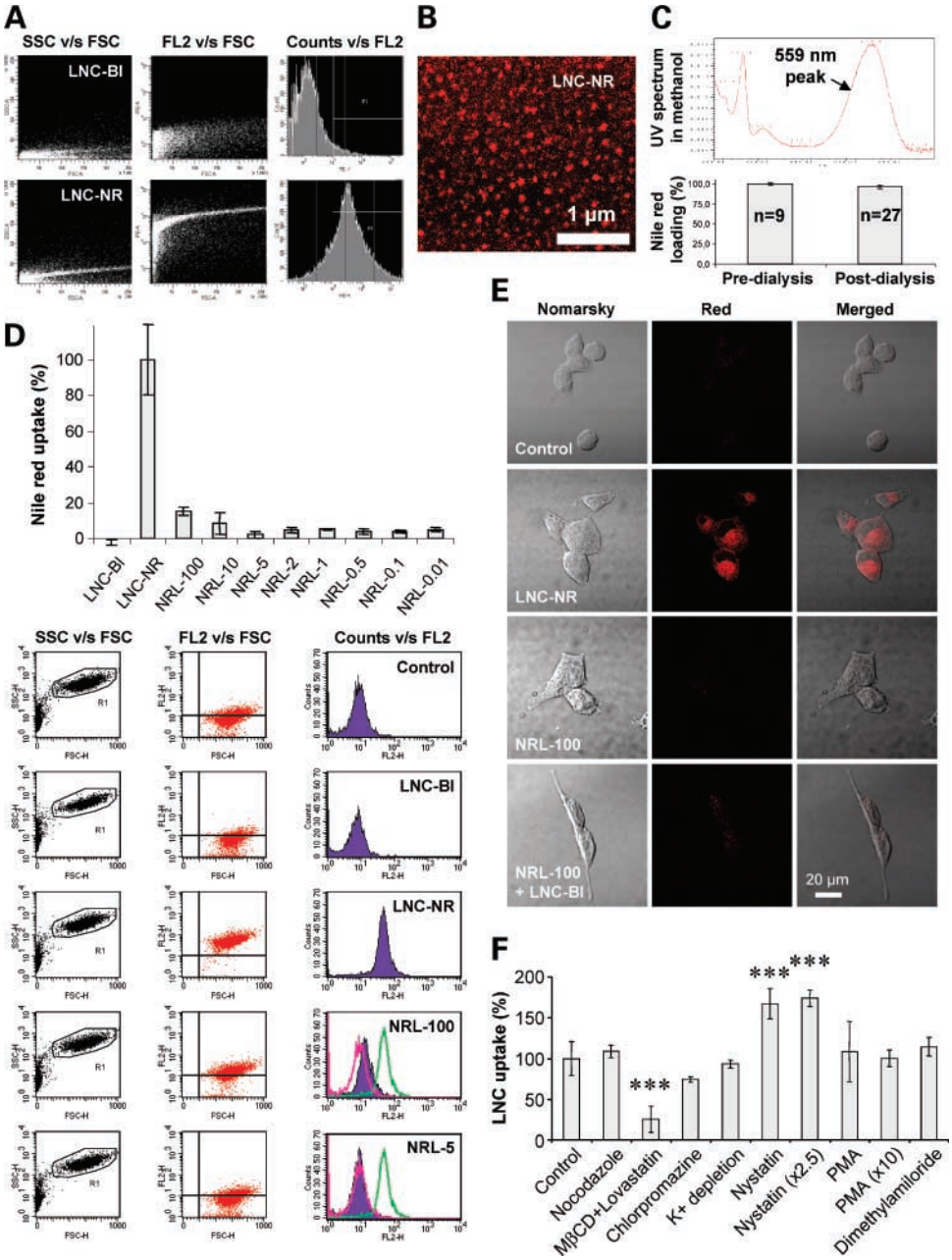

Figure 3. *In vitro* characterization of the internalization of Nile red–stained LNCs in F98 glioma cells. **A,** fluorescent-activated particle sorting of classical blank LNCs (LNC-Bl) and Nile red–stained LNCs (LNC-NR): analysis for granularity (side scatter) versus size (forward scatter; *SSC v/s FSC*), fluorescence intensity versus size (*FL2 v/s FSC*), and numbers versus fluorescence intensity (*Counts v/s FL2*). Note the dramatic increase in fluorescence intensity between LNC-Bl and LNC-NR and consecutive LNC number distribution. **B,** clusters of Nile red–stained LNCs are visualized by fluorescent microscopy. **C,** typical paclitaxel UV spectrum in methanol presenting an absorbance peak at 559 nm and HPLC quantification at 559 nm of remaining Nile red in the LNCs after 48 h of dialysis at 37°C in PBS (pH 7.4; post-dialysis) by comparison with initial loading (pre-dialysis). **D,** flow cytometry analysis of Nile red uptake by F98 cells after 2 h of incubation. For quantifications represented on the histogram, no treatment (*control*) and incubation with Nile red–loaded LNC (*LNC-NR*) were considered as to represent the 0% and 100% uptake of Nile red, respectively. For comparison, blank LNC (LNC-Bl) and solutions of free Nile red at final concentration varying from 5.88 ng/mL (NRL-100) to 0.588 pg/mL (NRL-0.01) that correspond to 100% and to 0.01% of the Nile red provided by LNC-NR, respectively, were incubated with F98 cells. Cell analysis was made for granularity versus size (*SSC v/s FSC*), fluorescence intensity versus size (*FL2 v/s FSC*), and numbers versus fluorescence intensity (*Counts v/s FL2*). Counts for control (*pink*) and LNC-NR (*green*) were included on panels representing those for NRL-100 and NRL-5. **E,** confocal laser scanning microscopy images (*Nomarsky, red*, and *merged*) after 10-min incubation of control (no treatment), LNC-NR, NRL-100, NRL-100, and LNC-Bl with F98 cells. Note (both in **D** and **E**) that only Nile red provided from LNC-NR was significantly internalized by F98 cells. **F,** variation of the basal mean fluorescence intensity of F98 cells after 2 h of incubation with Nile red–stained LNCs and treatment with known inhibitors of endocytosis. Note the strong inhibitory effect of methyl-β-cyclodextrin(*MβCD*) and lovastatin. ***, $P < 0.01$ (Dunnett's test).

mechanism that involve one or both of the two known cholesterol enriched membrane microdomains: lipid rafts and caveolae (referred to as a specialized form of invaginated lipid raft that contains caveolin-1; ref. 50). Hence, nystatin, which is a membrane-permeable cholesterol-binding drug that has been shown to selectively disrupt lipid rafts, caveolae structures, and block caveolae function while not affecting clathrin-coated pits, was used to sequestrate cholesterol (51–53). Surprisingly, treatment of F98 cells with nystatin (10 or 25 μg/mL) resulted in an increase of LNC uptake (Fig. 3F). In parallel, treatment of F98 cells with phorbol 12-myristate 13-acetate (1 and 10 μmol/L), which are activators of protein kinase C known to disrupt caveolae and block their invaginations (54), did not result in any reduction of LNC uptake by glioma cells, indicating no apparent direct role for caveolae-dependent mechanisms (Fig. 3F). Finally, treatment with dimethylamiloride, which is known to affect macropinocytosis (42), a mechanism that mainly contribute to antigen uptake by professional antigen-presenting cells, resulted in no effect as expected (Fig. 3F).

Characterization of Paclitaxel-Loaded LNCs and Their Effects on *In vitro* and *In vivo* Glioma Cell Growth

To further investigate the potential interest of the LNCs presented here, we aimed to prepare LNCs loaded with the MDR-sensitive substrate antineoplastic agent paclitaxel.

Paclitaxel was incorporated in LNCs with a high encapsulation rate (93.0 ± 3.1%, mean ± SD). Because, its stability was also confirmed through the heat cycles required to produce paclitaxel-loaded LNCs with 97.3% remaining intact drug, the initial amount of drug added during formulation was considered to be equal to final amount contained in paclitaxel-loaded LNC suspensions. Although the release profile of PEG-HS was primarily characterized by a burst effect, paclitaxel was released in a sustained fashion over a long time period (Fig. 4A). These data suggest the entrapment of paclitaxel inside the hydrophobic core of LNCs and support the fact that all lipophilic components are mainly hidden by the PEG steric barrier of the PEG-HS at the LNC interface (Fig. 4B).

To determine the potential interest of these nanocarriers in the treatment of cancer, LNCs were used in an *in vitro* glioma cell survival assay. After being applied on glioma cells, paclitaxel-loaded LNCs were shown to dramatically reduce cancer cell survival in comparison with paclitaxel alone (Taxol solution) with >100 times efficiency on 9L cells (Fig. 5A) and >1,000 times efficiency on F98 cells (Fig. 5B). Interestingly, Solutol on its own was not able to improve the effects of paclitaxel (Fig. 5A and B). To examine whether nontransformed cells were less sensitive to cell death induced by paclitaxel-loaded LNCs, the same assay was repeated on newborn rat astrocyte primary cultures. As shown on Fig. 5C, our data illustrate that such slowly dividing or nondividing cells are fairly insensitive to cell death induced by either paclitaxel solution or paclitaxel-loaded LNCs with no difference between these two treatments.

We further wanted to determine whether or not this cytotoxic effect resulted in significant improvement in tumor evolution *in vivo* by using an F98 s.c. glioma model that represented a straightforward way to evaluate the LNC influence on an MDR-expressing tumor. Whereas Taxol treatment showed no significant effect, paclitaxel-loaded LNC treatment was able to significantly lower both tumor mass (Fig. 5D) and tumor volume evolution (Fig. 5E). Interestingly, in a similar fashion to what was found *in vitro* in the F98 model, the addition of Solutol HS15 at the same concentration to the one contained in LNCs did not result in any improvement in tumor evolution. This proves the importance of the nanocarrier itself for the association of an antitumor effect to MDR reversion. We conclude, therefore, that paclitaxel-loaded LNCs may represent a potent tool in the treatment of glioma *in vivo*.

Discussion

This study showed that the overall effect of LNCs is to substantially optimize the bioavailability of anticancer drug while at the same time overcoming MDR mechanisms. Relating to the parenteral delivery of paclitaxel, one of the most promising drugs currently available for cancer

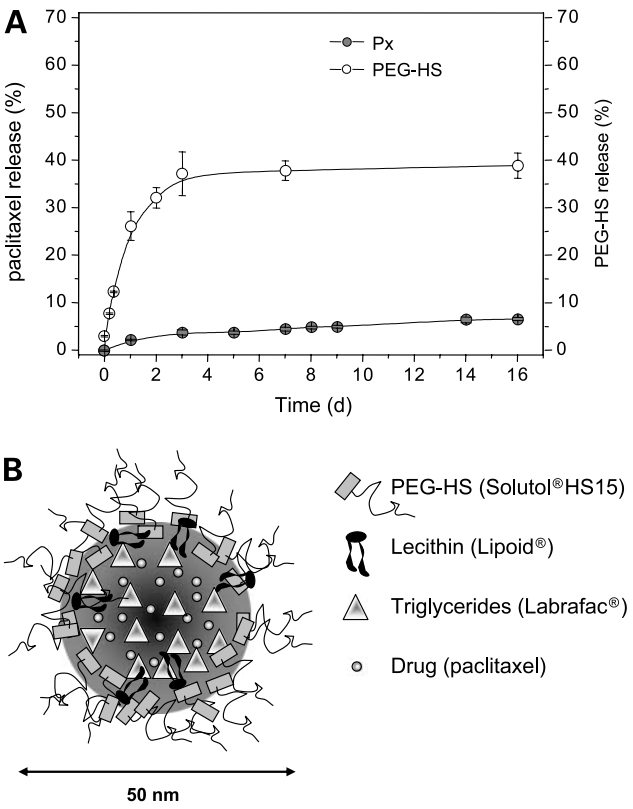

Figure 4. Characterization of paclitaxel-loaded LNCs. **A**, *in vitro* drug and surfactant release profiles from LNCs in phosphate buffer (0.625 mg/mL paclitaxel loading). **B**, schematic representation of paclitaxel-loaded LNCs showing a topographic distribution of the hydrophobic drug in the internal lipid core and nonionic PEG-HS chains (Solutol HS 15) at the interface. *Px*, paclitaxel; *PEG-HS*, Solutol HS15.

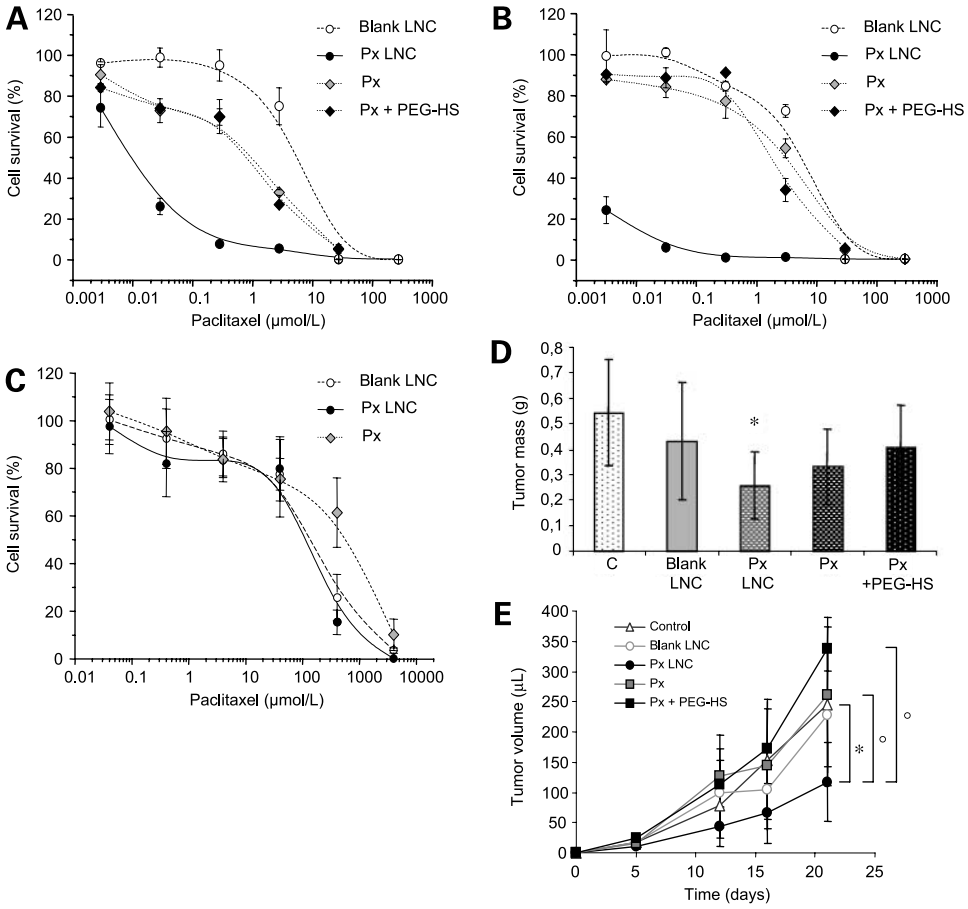

Figure 5. Effects of paclitaxel-loaded LNCs on glioma cell growth. **A** to **C**, *in vitro* effects of paclitaxel-loaded LNCs on the survival of 9L (**A**), F98 (**B**), and newborn rat primary astrocytes (**C**). *Px LNC,* paclitaxel-loaded LNCs; *Px,* Taxol alone; *Px + PEG-HS,* Taxol and Solutol HS15; *blank LNC,* unloaded LNCs. Total paclitaxel concentration per well was the same for paclitaxel, paclitaxel LNC, and paclitaxel + PEG-HS as confirmed by HPLC measurements (cf. paclitaxel stability and drug loading). Note the weak efficacy of Taxol formulation for reducing cell growth in both 9L (**A**) and F98 (**B**) model when compared with paclitaxel-loaded nanocapsules. In parallel, paclitaxel-loaded LNCs showed no significant effect on cell survival when applied to slowly dividing nontransformed cells (**C**). **D** and **E**, *in vivo* effects of paclitaxel-loaded LNC treatment on the growth of F98 glioma cells implanted s.c. Total paclitaxel dose (2.5 mg/kg body weight) was the same for C, paclitaxel LNC, and paclitaxel + PEG-HS. Note that tumor growth assessed by tumor mass in (**D**) and tumor size measurements in (**E**), with statistics on day 21, was significantly reduced by paclitaxel-loaded LNCs, whereas the commercially available Taxol formulation had smaller effects. *C,* control; *Px-LNC,* paclitaxel-loaded LNC; *Px,* Taxol only; *Px + PEG-HS,* Taxol with Solutol HS15 solution. *Points,* mean; *bars,* SD. *, $P < 0.05$ (Dunnett's test). Statistical analysis by pairs also show significant differences in **E** on day 21 between paclitaxel LNC and paclitaxel as well as paclitaxel LNC and paclitaxel + PEG-HS. °, $P < 0.05$ (Fisher's test).

therapy (55–57), the nanocarrier system described here presents three main advantages. First, it allows a drug sustained release, a point of major importance because it has been reported that cancer cell sensitivity to paclitaxel concentration increases significantly with the increasing duration of exposure to the drug *in vitro* due to an increased probability of arresting the cell cycle during the late G_2 or M phase (56, 57). Second, LNCs are obtained without the use of Cremophor-EL, the nonionic surfactant in the Taxol formulation that displays a wide variety of intrinsic toxic side effects that limit the amount of drug that can be safely given (58). Third, LNCs target the intracellular compartment in which they likely represent stable drug reservoirs (27). Indeed, whereas hydrophobic compounds may diffuse into interstitial spaces, they showed little accumulation in tumor cells. Thus, the presence of LNCs in the glioma cytosolic spaces would allow paclitaxel to be released in the close vicinity of the microtubule network on which it is acting.

In parallel to improving hydrophobic drug bioavailability through the optimization of drug formulation and targeting, the dual interest of LNCs is to reduce MDR phenomena, thus decreasing paclitaxel clearance. The reversion of multidrug resistance in tumor cells has already been observed with antitumoral drugs encapsulated in colloidal carriers, such as liposomes, polymer nanoparticles, or block copolymer micelles. Thus, several mechanisms of reversion have been proposed (2, 15–21). The local delivery of the drug in high concentration close to the cell membrane would affect the local microconcentration of the

drug and is supposed to be able to saturate MDR efflux pumps. Simultaneous drug release and polymer degradation, with a particular attention being paid to the nature of the wall polymer used proved to be of prime importance. The formation of an ion pair between polycyanoacrylic acid, resulting from the degradation of the wall material, and doxorubicin was shown to improve drug diffusion across the plasma membrane and to reduce drug recognition as P-glycoprotein substrate. However, such a system raises the problem of the integrity of the drug and the persistence of its cytotoxic activity (2). In addition, it was shown that block copolymer micelles decrease intracellular ATP levels together with reducing ATPase activity of P-glycoprotein (22, 59). In all cases, a physical interaction between the structure of the nanocarrier and the efflux transporter itself has been excluded. Alternatively, it has been shown that the coencapsulation of a reversing agent (cyclosporine A) with doxorubicin inhibits MDR (2). However, one has to be careful with the use of compounds, termed chemosensitizers or reversing agents (e.g., verapamil, quinidine, and amiodarone) because *in vivo* application of most of these compounds is precluded by side effects (13).

Concerning the LNCs presented here, experiments using P-glycoprotein–enriched inside-out vesicles and confocal laser scanning microscopy imaging studies support an intracellular interaction of the LNCs with P-glycoprotein–related efflux pumps. Although this observation does not exclude external MDR inhibition, it suggests that LNCs allow not only a genuine intracellular release of paclitaxel but also an intracellular-driven MDR inhibition. As intrinsic MDR-blocking activity of Solutol HS15 turned out to be inefficient after 24 hours on F98 cells *in vivo*, most of the ''long-term'' MDR reversion we observed must be directly attributed to the LNC carrier system itself. In parallel, our flow cytometric studies showed, collectively, a major sensitivity of the LNC uptake process to cholesterol perturbation in glioma cells. However, cholesterol depletion (methyl-β-cyclodextrin and lovastatin) and cholesterol sequestration (nystatin) seemed to have opposite effects (Fig. 3F). This assumption must be ascribed to convoluted roles of nystatin that not only can bind nonesterified cholesterol but also create transmembrane pores and alter cell membrane permeability (60). Consequently, even with a major role for cholesterol, nystatin may influence positively LNC internalization in glioma cells. As clathrin-dependent endocytosis seemed to be weakly involved in LNC internalization, cholesterol-rich microdomains unresponsive to protein kinase C activation (e.g., a subpopulation of lipid rafts) were suspected to play the key role. It is interesting to note that for the same particle size (50 nm), LNC intracellular internalization differed from the one of fluorescent polystyrene spheres that involved clathrin-coated pits (61). Assuming that uptake mechanisms are likely to be cell specific, not only the size but also the nature of the internalized particles must be equally important. Thus, we here propose a mechanism by which LNC uptake together with consecutive intracellular cholesterol movements would constitute the core of the LNC inhibitory effects on MDR (Fig. 6). It has indeed recently been shown that cholesterol itself modulates positively P-glycoprotein activity (62) and that caveolins, which are highly concentrated in nondisrupted caveolae, negatively (63). According to this, LNC inhibitory effects on efflux pumps would be partially direct, through the progressive release of intracellular free PEG-HS that interacts with MDR efflux pumps and reduce their activity, and mainly indirect, through redistribution of intracellular cholesterol (Fig. 6). The resulting increase in cytosolic paclitaxel concentrations would itself lead to cell death (Fig. 6).

In conclusion, LNCs combined the specific advantages of block copolymer micelles, with an unprecedented *in vitro* toxicity up to 1,000-fold higher than that of the free drug that must be linked to rapid cell internalization (15–18), and those of poly(alkyl cyanoacrylate) nanoparticles, with the possibility to graft a molecular recognition moiety to their surface to achieve tissue and even subcellular targeting (19–21). As different efflux pumps are frequently coexpressed by cancer cells and often induced by the treatment itself with many derivations from the original transformed cell, the use of LNCs as a new MDR-inhibiting system present the other particularity of probably not being highly selective to a specific efflux

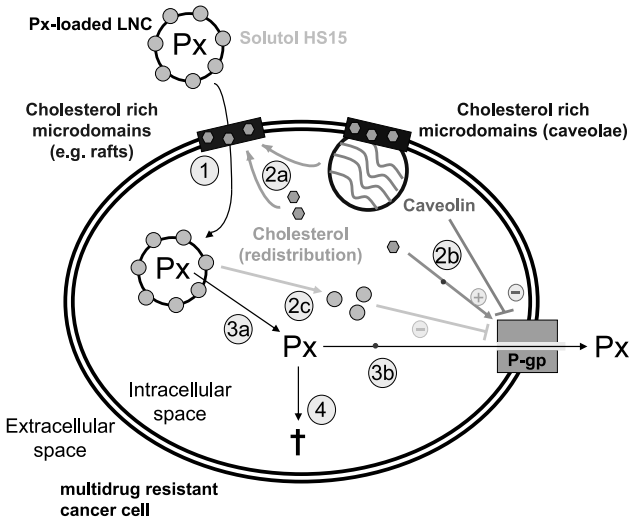

Figure 6. Model explaining the effects of paclitaxel-loaded LNCs on MDR and cancer cell growth. Uptake of paclitaxel-loaded LNCs in the intracellular space of cancer cells seems to involve cholesterol-rich microdomains, among which subpopulations of lipid rafts are potential candidates (*1*). Consecutive intracellular cholesterol redistribution (*2a*) may interfere with other cholesterol-rich microdomains resulting in a down-regulation of P-glycoprotein activity (*2b*; e.g., positive effects of cholesterol blocked and negative effects of caveolin accentuated). Alternatively, inhibition of MDR can result from Solutol HS15 effects after release from LNCs in the intracellular space (*2c*). Paclitaxel itself would be released in a close vicinity to the microtubule network on which it is active (*3a*), with reduction of its efflux as a consequence of the inhibition of the P-glycoprotein activity (*3b*). Thus, the overall adjuvant effect of LNCs would result in an improvement of paclitaxel intracellular bioavailability (*4*) and in an increase of tumor cell death (†).

pump but being able to act on the overall classic MDR mechanism. The development of such nanocarrier systems, therefore, requires attention and further investigations toward the application of new therapeutic protocols in humans, including mini-invasive stereotaxic treatments of deep cerebral tumors.

Acknowledgments

We thank Dr. Richard Milner (The Scripps Research Institute, La Jolla, CA) for critical reading of the article. We are also grateful to Drs. Franck Lacoeuille and Jean-Michel Oger (Institut National de la Sante et de la Recherche Medicale Unité 646, Angers, France), Pierre Legras and Jérôme Roux (Service Commun d'Animalerie Hospitalo-Universitaire, Angers, France), Robert Filmon and Romain Mallet (Service Commun d'Imagerie et d'Analyses Microscopiques, Angers, France), and Dr. Catherine Guillet (Service Commun de Cytometrie et d'Analyse Nucléotidique, Angers, France) for skillful technical support.

References

1. Kreuter J. Nanoparticulate systems for brain delivery of drugs. Adv Drug Deliv Rev 2001;47:65 – 81.

2. Brigger I, Dubernet C, Couvreur P. Nanoparticles in cancer therapy and diagnosis. Adv Drug Deliv Rev 2002;54:631 – 51.

3. Sells RA, Owen RR, New RR, Gilmore IT. Reduction in toxicity of doxorubicin by liposomal entrapment. Lancet 1987;2:624 – 5.

4. Rahman A, Treat J, Roh JK, et al. A phase I clinical trial and pharmacokinetic evaluation of liposome-encapsulated doxorubicin. J Clin Oncol 1990;8:1093 – 100.

5. Cowens JW, Creaven PJ, Greco WR, et al. Initial clinical (phase I) trial of TLC D-99 (doxorubicin encapsulated in liposomes). Cancer Res 1993; 53:2796 – 802.

6. Gabizon A, Catane R, Uziely B, et al. Prolonged circulation time and enhanced accumulation in malignant exudates of doxorubicin encapsulated in polyethylene-glycol coated liposomes. Cancer Res 1994; 54:987 – 92.

7. Storm G, ten Kate MT, Working PK, Bakker-Woudenberg IA. Doxorubicin entrapped in sterically stabilized liposomes: effects on bacterial blood clearance capacity of the mononuclear phagocyte system. Clin Cancer Res 1998;4:111 – 5.

8. Gref R, Minamitake Y, Peracchia MT, Trubetskoy V, Torchilin V, Langer R. Biodegradable long-circulating polymeric nanospheres. Science 1994; 263:1600 – 3.

9. Couvreur P, Barratt G, Fattal E, Legrand P, Vauthier C. Nanocapsule technology: a review. Crit Rev Ther Drug Carrier Syst 2002;19:99 – 134.

10. Muller RH, Keck CM. Challenges and solutions for the delivery of biotech drugs: a review of drug nanocrystal technology and lipid nanoparticles. J Biotechnol 2004;113:151 – 70.

11. Gottesman MM, Fojo T, Bates SE. Multidrug resistance in cancer: role of ATP-dependent transporters. Nat Rev Cancer 2002;2:48 – 58.

12. Juliano RL, Ling V. A surface glycoprotein modulating drug permeability in Chinese hamster ovary cell mutants. Biochim Biophys Acta 1976;455:152 – 62.

13. Varma MV, Ashokraj Y, Dey CS, Panchagnula R. P-glycoprotein inhibitors and their screening: a perspective from bioavailability enhancement. Pharmacol Res 2003;48:347 – 59.

14. Mayer LD, Shabbits JA. The role for liposomal drug delivery in molecular and pharmacological strategies to overcome multidrug resistance. Cancer Metastasis Rev 2001;20:87 – 93.

15. Batrakova EV, Li S, Alakhov VY, Elmquist WF, Miller DW, Kabanov AV. Sensitization of cells overexpressing multidrug-resistant proteins by pluronic P85. Pharm Res 2003;20:1581 – 90.

16. Batrakova EV, Zhang Y, Li Y, et al. Effects of pluronic P85 on GLUT1 and MCT1 transporters in the blood-brain barrier. Pharm Res 2004;21: 1993 – 2000.

17. Batrakova E, Lee S, Li S, Venne A, Alakhov V, Kabanov A. Fundamental relationships between the composition of pluronic block copolymers and their hypersensitization effect in MDR cancer cells. Pharm Res 1999;16:1373 – 9.

18. Ramaswamy M, Zhang X, Burt HM, Wasan KM. Human plasma distribution of free paclitaxel and paclitaxel associated with diblock copolymers. J Pharm Sci 1997;86:460 – 4.

19. Vauthier C, Dubernet C, Chauvierre C, Brigger I, Couvreur P. Drug delivery to resistant tumors: the potential of poly(alkyl cyanoacrylate) nanoparticles. J Control Release 2003;93:151 – 60.

20. Soma CE, Dubernet C, Bentolila D, Benita S, Couvreur P. Reversion of multidrug resistance by co-encapsulation of doxorubicin and cyclosporin A in polyalkylcyanoacrylate nanoparticles. Biomaterials 2000;21:1 – 7.

21. Hu YP, Jarillon S, Dubernet C, Couvreur P, Robert J. On the mechanism of action of doxorubicin encapsulation in nanospheres for the reversal of multidrug resistance. Cancer Chemother Pharmacol 1996; 37:556 – 60.

22. Batrakova EV, Li S, Vinogradov SV, Alakhov VY, Miller DW, Kabanov AV. Mechanism of pluronic effect on P-glycoprotein efflux system in blood-brain barrier: contributions of energy depletion and membrane fluidization. J Pharmacol Exp Ther 2001;299:483 – 93.

23. Coon JS, Knudson W, Clodfelter K, Lu B, Weinstein RS. Solutol HS 15, nontoxic polyoxyethylene esters of 12-hydroxystearic acid, reverses multidrug resistance. Cancer Res 1991;51:897 – 902.

24. Buckingham LE, Balasubramanian M, Emanuele RM, Clodfelter KE, Coon JS. Comparison of Solutol HS 15, Cremophor EL and novel ethoxylated fatty acid surfactants as multidrug resistance modification agents. Int J Cancer 1995;62:436 – 42.

25. Heurtault B, Saulnier P, Pech B, Proust JE, Benoit JP. A novel phase inversion-based process for the preparation of lipid nanocarriers. Pharm Res 2002;19:875 – 80.

26. Heurtault B, Saulnier P, Pech B, Proust JE, Benoit JP. Properties of polyethylene glycol 660 12-hydroxy stearate at a triglyceride/water interface. Int J Pharm 2002;242:167 – 70.

27. Heurtault B, Saulnier P, Pech B, Proust JE, Benoit JP. Physico-chemical stability of colloidal lipid particles. Biomaterials 2003;24: 4283 – 300.

28. Sun H, Dai H, Shaik N, Elmquist WF. Drug efflux transporters in the CNS. Adv Drug Deliv Rev 2003;55:83 – 105.

29. Coudore F, Authier N, Guillaume D, Beal A, Duroux E, Fialip J. High-performance liquid chromatographic determination of paclitaxel in rat serum: application to a toxicokinetic study. J Chromatogr B Biomed Sci Appl 1999;721:317 – 20.

30. Peltier S, Oger J, Lagarce F, Couet W, Benoît J. Enhanced oral paclitaxel bioavailability after administration of paclitaxel-loaded lipid nanocapsules. Pharm Res. In press.

31. McCarthy KD, de Vellis J. Preparation of separate astroglial and oligodendroglial cell cultures from rat cerebral tissue. J Cell Biol 1980;85: 890 – 902.

32. Greenspan P, Mayer EP, Fowler SD. Nile red: a selective fluorescent stain for intracellular lipid droplets. J Cell Biol 1985;100:965 – 73.

33. Lamprecht A, Benoit JP. Simple liquid-chromatographic method for Nile Red quantification in cell culture in spite of photobleaching. J Chromatogr B Analyt Technol Biomed Life Sci 2003;787:415 – 9.

34. Hed J, Hallden G, Johansson SG, Larsson P. The use of fluorescence quenching in flow cytofluorometry to measure the attachment and ingestion phases in phagocytosis in peripheral blood without prior cell separation. J Immunol Methods 1987;101:119 – 25.

35. Vasquez RJ, Howell B, Yvon AM, Wadsworth P, Cassimeris L. Nanomolar concentrations of nocodazole alter microtubule dynamic instability *in vivo* and *in vitro*. Mol Biol Cell 1997;8:973 – 85.

36. Zuhorn IS, Visser WH, Bakowsky U, Engberts JB, Hoekstra D. Interference of serum with lipoplex-cell interaction: modulation of intracellular processing. Biochim Biophys Acta 2002;1560:25 – 36.

37. Rodal SK, Skretting G, Garred O, Vilhardt F, van Deurs B, Sandvig K. Extraction of cholesterol with methyl-beta-cyclodextrin perturbs formation of clathrin-coated endocytic vesicles. Mol Biol Cell 1999;10:961 – 74.

38. Ohtani Y, Irie T, Uekama K, Fukunaga K, Pitha J. Differential effects of alpha-, beta- and gamma-cyclodextrins on human erythrocytes. Eur J Biochem 1989;186:17 – 22.

39. Larkin JM, Brown MS, Goldstein JL, Anderson RG. Depletion of intracellular potassium arrests coated pit formation and receptor-mediated endocytosis in fibroblasts. Cell 1983;33:273 – 85.

40. Wang LH, Rothberg KG, Anderson RG. Mis-assembly of clathrin lattices on endosomes reveals a regulatory switch for coated pit formation. J Cell Biol 1993;123:1107 – 17.

41. Anderson HA, Chen Y, Norkin LC. Bound simian virus 40 translocates to caveolin-enriched membrane domains, and its entry is inhibited by drugs that selectively disrupt caveolae. Mol Biol Cell 1996;7:1825 – 34.

42. Liu NQ, Lossinsky AS, Popik W, et al. Human immunodeficiency virus type 1 enters brain microvascular endothelia by macropinocytosis dependent on lipid rafts and the mitogen-activated protein kinase signaling pathway. J Virol 2002;76:6689 – 700.

43. Jordan JP, Hand CM, Markowitz RS, Black P. Test for chemotherapeutic sensitivity of cerebral gliomas: use of colorimetric MTT assay. J Neurooncol 1992;14:19 – 35.

44. Fournier E, Passirani C, Montero-Menei C, et al. Therapeutic effectiveness of novel 5-fluorouracil-loaded poly(methylidene malonate 2.1.2)-based microspheres on F98 glioma-bearing rats. Cancer 2003;97: 2822 – 9.

45. Piwnica-Worms D, Chiu ML, Budding M, Kronauge JF, Kramer RA, Croop JM. Functional imaging of multidrug-resistant P-glycoprotein with an organotechnetium complex. Cancer Res 1993;53:977 – 84.

46. Nabi IR, Le PU. Caveolae/raft-dependent endocytosis. J Cell Biol 2003;161:673 – 7.

47. Nichols B. Caveosomes and endocytosis of lipid rafts. J Cell Sci 2003;116:4707 – 14.

48. Pichler H, Riezman H. Where sterols are required for endocytosis. Biochim Biophys Acta 2004;1666:51 – 61.

49. Johannes L, Lamaze C. Clathrin-dependent or not: is it still the question? Traffic 2002;3:443 – 51.

50. Matveev S, Li X, Everson W, Smart EJ. The role of caveolae and caveolin in vesicle-dependent and vesicle-independent trafficking. Adv Drug Deliv Rev 2001;49:237 – 50.

51. Rothberg KG, Heuser JE, Donzell WC, Ying YS, Glenney JR, Anderson RG. Caveolin, a protein component of caveolae membrane coats. Cell 1992;68:673 – 82.

52. Lisanti MP, Tang ZL, Sargiacomo M. Caveolin forms a hetero-oligomeric protein complex that interacts with an apical GPI-linked protein: implications for the biogenesis of caveolae. J Cell Biol 1993; 123:595 – 604.

53. Ros-Baro A, Lopez-Iglesias C, Peiro S, et al. Lipid rafts are required for GLUT4 internalization in adipose cells. Proc Natl Acad Sci U S A 2001;98: 12050 – 5.

54. Smart EJ, Foster DC, Ying YS, Kamen BA, Anderson RG. Protein kinase C activators inhibit receptor-mediated potocytosis by preventing internalization of caveolae. J Cell Biol 1994;124:307 – 13.

55. Brandes AA, Pasetto LM, Monfardini S. New drugs in recurrent high grade gliomas. Anticancer Res 2000;20:1913 – 20.

56. Cahan MA, Walter KA, Colvin OM, Brem H. Cytotoxicity of taxol *in vitro* against human and rat malignant brain tumors. Cancer Chemother Pharmacol 1994;33:441 – 4.

57. Horwitz SB. Taxol (paclitaxel): mechanisms of action. Ann Oncol 1994;5 Suppl 6:S3 – 6.

58. Dorr RT. Pharmacology and toxicology of Cremophor EL diluent. Ann Pharmacother 1994;28:S11 – 4.

59. Batrakova EV, Li S, Elmquist WF, Miller DW, Alakhov VY, Kabanov AV. Mechanism of sensitization of MDR cancer cells by Pluronic block copolymers: selective energy depletion. Br J Cancer 2001; 85:1987 – 97.

60. Coutinho A, Silva L, Fedorov A, Prieto M. Cholesterol and ergosterol influence nystatin surface aggregation: relation to pore formation. Biophys J 2004;87:3264 – 76.

61. Rejman J, Oberle V, Zuhorn IS, Hoekstra D. Size-dependent internalization of particles via the pathways of clathrin- and caveolae-mediated endocytosis. Biochem J 2003;377:159 – 69.

62. Troost J, Lindenmaier H, Haefeli WE, Weiss J. Modulation of cellular cholesterol alters P-glycoprotein activity in multidrug-resistant cells. Mol Pharmacol 2004;66:1332 – 9.

63. Jodoin J, Demeule M, Fenart L, et al. P-glycoprotein in blood-brain barrier endothelial cells: interaction and oligomerization with caveolins. J Neurochem 2003;87:1010 – 23.

Molecular Cancer Therapeutics

A new generation of anticancer, drug-loaded, colloidal vectors reverses multidrug resistance in glioma and reduces tumor progression in rats

Emmanuel Garcion, Alf Lamprecht, Béatrice Heurtault, et al.

Mol Cancer Ther 2006;5:1710-1722.